CYCLE-BY-CYCLE COMBUSTION VARIATIONS IN SPARK-IGNITED ENGINES

C.S. DAW
Engineering Technology Division, Oak Ridge National Laboratory, Oak Ridge TN 37831-8088 USA
C.E.A. FINNEY
College of Engineering, University of Tennessee, Knoxville TN 37996-2210 USA
M.B. KENNEL
Institute for Nonlinear Science, University of California, San Diego, La Jolla CA 92093-0402 USA
and
F.T. CONNOLLY
Ford Motor Company, Dearborn MI 48121-2053 USA

ABSTRACT

Under constant nominal operating conditions, internal combustion engines can exhibit substantial variation in combustion efficiency from one cycle to the next. Previous researchers have attempted to explain these variations as resulting from stochastic, linear, or chaotic physical processes. Our investigations indicate that cyclic combustion variations can be explained as the result of interactions between a global low-dimensional nonlinearity and small-scale, high-dimensional processes that perturb the nonlinearity. Using this approach, we have proposed a simple model that accurately simulates experimentally observed patterns in cyclic combustion variations. Our model also explains the apparent discrepancies among previous investigators regarding the basic nature of cyclic variations. Further, it appears that symbolic time series analysis is useful for characterizing the observed model and experimental behavior.

1 Introduction

Under constant nominal operating conditions, internal combustion engines can exhibit substantial variation from one cycle to the next in combustion efficiency (*i.e.*, the fraction of fuel energy released by combustion). This phenomenon has been observed and studied since at least the 19th century (*e.g.*, Clerk [1]), and recent studies have been numerous [2, 3, 4, 5, 6, 7, 8, 9]. Extensive reviews are given by [11, 12].

Concerns about *cyclic variability* (CV) are highly relevant today because economic and regulatory pressures are pushing engine manufacturers to design engines that are particularly prone to this problem. For example, there is a trend to operate automotive engines with lean fueling and exhaust-gas recirculation (EGR) to increase fuel economy and minimize $\mathrm{NO_x}$ emissions. CV occurs more frequently with lean fueling and EGR and actually limits the potential benefits which can be derived from these operating modes.

Previous researchers have characterized CV in wide-ranging and sometimes apparently contradictory terms. For example, some describe the phenonmenon as strictly stochastic, while others report linear correlations over time [2, 6, 7, 10]. Still others have proposed that chaotic dynamics are involved [3, 9, 13]. These apparently contradictory experimental observations have created a continuing debate in the engineering community about the true nature of CV.

In this article we present results supporting the conclusion that CV can be explained as the result of a simple, nonlinear mapping that is perturbed by high-dimensional (*i.e.*, stochastic) effects. Based on physical arguments, we believe that the largest stochastic

effects occur as the result of fluctuations in the effective values of deterministic parameters. Our approach to modeling the deterministic mapping is greatly simplified in that we are only concerned with variations in the global combustion patterns integrated over the combustion phase of each cycle. We do not attempt to simulate spatial details and instead focus on the cylinder-average mass balance and energy release. The resulting combustion time series predictions look remarkably similar to those observed with our experimental engines. Because our model is physically realistic, we expect that it can be used to predict CV trends with engine design changes and to develop real-time feedback control.

2 The Four-Stroke Engine Cycle

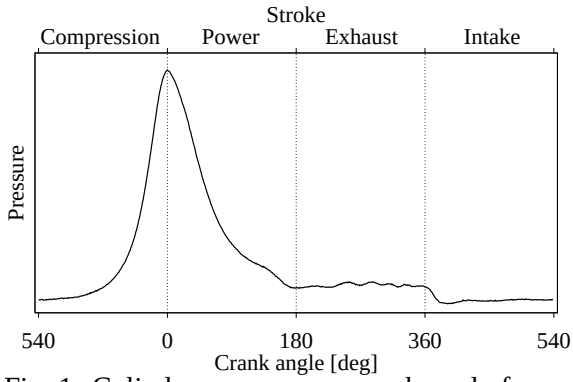

Fig. 1: Cylinder pressure vs. crank angle for one engine cycle.

Most gasoline-fueled engines operate with the four-stroke, spark-ignition (Otto) cycle. Initially, fuel and air are inducted through the intake valve into the cylinder and the resulting mixture compressed. Near maximum compression, a high-voltage spark produces ignition. Combustion and expansion of the hot gases produce work, which is transferred through the piston and crankshaft to the load (*e.g.*, wheels in automobiles). As the piston moves upward again following the power stroke, exhaust gases vent through the exhaust valve. Following exhaust, fresh fuel and air are added to begin the next cycle.

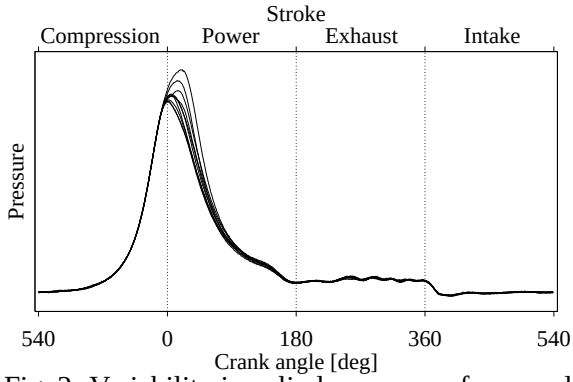

Fig. 2: Variability in cylinder pressure from cycle to cycle, viewed over 10 consecutive cycles.

In actuality, not all of the combustion product gases are expelled during the exhaust stroke. Because of engine design constraints, this *residual fraction* is higher at idling or low engine speeds than at high engine speeds. The residual gases contain combustion product as well as unreacted fuel and air which can influence the initial conditions for the next combustion.

It is common practice to describe piston location in terms of *crank angle degrees* (CAD), which describes the angle of the crankshaft relative to *top dead center*, where the piston is at its furthest position into the cylinder. As depicted in Fig. 1, the course of each combustion event can be followed by monitoring the internal cylinder pressure vs. crank angle. As combustion proceeds, cylinder pressure exceeds that which would occur without combustion, thereby producing useful work. Pressure traces during CV become non-repeating as shown in Fig. 2.

As illustrated in Fig. 3, the occurrence of CV can produce dramatic effects on engine output. In the series (i), which represents typical operation for near-stoichiometric fueling, the variation in combustion heat release from cycle to cycle is less than one percent of the average value. Series (ii) and (iii) illustrate typical high CV operation at lean fueling conditions. Some combustion events leave residual unburned fuel, whereas others produce excess energy because of the combustion of residual and fresh fuel. Both combustion extremes are undesirable because they produce alternating pulses of fuel and nitrogen oxides in the exhaust and perceivable "roughness".

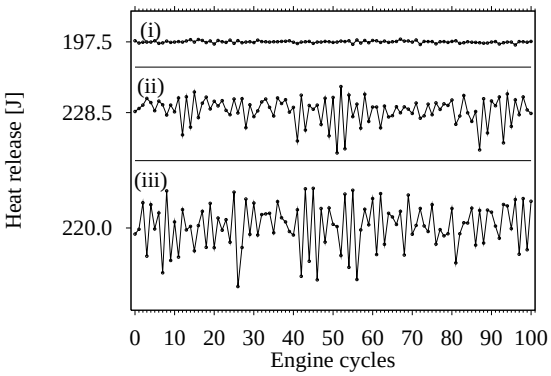

Fig. 3: Engine heat-release sequences at nominal operating conditions for $\phi_\circ = 0.91$ (i), 0.59 (ii) and 0.53 (iii). Means are shifted, but vertical scales are equal.

3 Model development

3.1 *Combustion nonlinearity*

To model CV we concentrate on the residual-gas effect as the dominant deterministic component. Because residual gas contains unburned oxygen and fuel from preceding cycles, it influences the overall average composition of the cyclinder gas at the time of spark.

Figure 4 illustrates why small changes in gas composition can have extremely large effects on combustion rate at lean conditions. In this figure we see that as the *equivalence ratio* (ratio of fuel present relative to fuel required to consume all oxygen) reduces below a critical value, the burning rate decreases exponentially. Here, burning rate is indicated by *laminar flame speed*, the speed at which a flame propagates through a quiescent mixture. This critical equivalence ratio is often referred to in combustion literature as the *lean flammability limit*. For hydrocarbon fuels, the lean flammability limit is typically about 0.5 – 0.6 [14]. There is a similar point at high equivalence ratios which is referred to as the *rich flammability limit*. Both limits represent conditions at which burning rate becomes so slow that heat generation is less than heat dissipation, and the flame extinguishes.

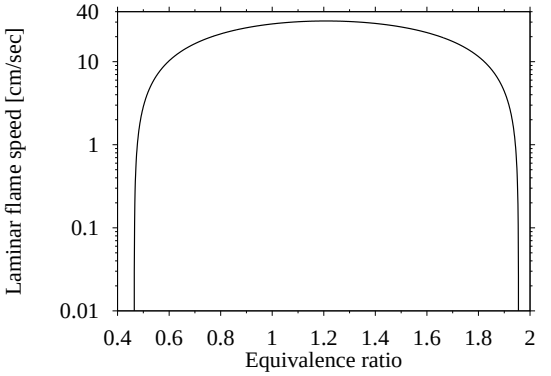

Fig. 4: Variation of laminar flame speed for gasoline in air at 300 K (from [15]).

In the highly turbulent conditions inside the engine cylinder we do not expect that combustion will proceed exactly the same as it does under laminar flow or quiescent conditions. Nevertheless, we do expect that the degree of combustion completion will also tend to drop

exponentially as the average fuel-air ratio at the time of spark is decreased below a critical value. To model this nonlinearity, we define the combustion efficiency C in any given cycle is defined as the fraction of the fuel present that burns. We next define a specific functional form for the effect of gas composition on combustion efficiency:

$$C[n] = C(\Phi[n]) = C_{\max}\left[1 + 100^{-\frac{\Phi[n]-\phi_{\mathrm{m}}}{\phi_{\mathrm{u}}-\phi_{\mathrm{l}}}}\right]^{-1}, \tag{1}$$

where $\Phi[n] = m[n]/(Ra[n])$ is the in-cylinder equivalence ratio at the time of spark, and R is the mass of air required to burn a unit mass of fuel (a constant). Thus if $m[n]$ and $a[n]$ are known at the time of spark, the outcome of the combustion ($C[n]$) can be determined.

As represented by Eq. 1, the relationship between combustion efficiency and equivalence ratio has a sigmoidal shape, converging to $C_{\max}$ (near 1) as Φ approaches stoichiometry (*i.e.*, $\Phi = 1$) and converging to 0 as Φ gets very small. This relationship is strictly empirical but it exhibits the expected exponential decay of combustion below a critical equivalence ratio as well as satisfying the obvious limiting constraints for combustion efficiency. We parameterize the sigmoid by ϕ_{l} and ϕ_{u}, conditions where efficiency is approximately 10% and 90% of $C_{\max}$, defining $\phi_{\mathrm{m}} = (\phi_{\mathrm{u}} + \phi_{\mathrm{l}})/2$. Here we only consider lean combustion ($\Phi < 1$), where the primary interest in cyclic variablity lies.

The above expression for combustion efficiency ignores inert combustion products which may be in the cylinder, but these can be easily added. Temperature, which is also known to affect burning rate, can also be added as a factor in the combustion efficiency function. For the experimental results described later, it appears that the effects of both inert combustion products and temperature are relatively minor.

3.2 *Discrete mass balances*

To complete the deterministic part of our model, we include the nonlinear combustion term in discrete cyclic mass balances for fuel and air. The result is a two-dimensional dynamic map relating the masses of fuel and air present before spark in cycle n to the same quantities in cycle $n + 1$:

$$m[n+1] = m_{\mathrm{f}}(1-F) + F(1-C[n])m[n], \tag{2}$$

$$a[n+1] = a_{\mathrm{f}}(1-F) + RF(1-C[n])a[n], \tag{3}$$

where m is the mass of fuel in the cylinder at the time of spark, a is the mass of air in the cylinder at the time of spark, F is the fraction of cylinder gas retained as residuals, m_{f} is the air mass injected into the cylinder when $F = 0$, and a_{f} is the fuel mass injected into the cylinder when $F = 0$.

There is an additional constraint on the mass balance because the total number of moles in the cylinder at the beginning of each cycle is fixed by the cylinder volume and intake temperature and pressure. At constant intake conditions and ignoring combustion products, this constraint can be written as

$$n_T = \frac{m[n]}{W_{\mathrm{f}}} + \frac{a[n]}{W_{\mathrm{a}}}, \tag{4}$$

where n_T is the total gas moles in the cylinder (fixed by the ideal gas law), W_f is the molecular weight of the fuel, and W_a is the molecular weight of air.

Because of this second constraint, the mapping is effectively one-dimensional, and in principle, could be written as

$$m[n+1] = g(m[n]), \tag{5}$$

where g is the effective 1-D mapping function. Because the fuel mass is typically not readily measureable, it is more useful to write the latter as

$$Q[n+1] = g'(Q[n]), \tag{6}$$

where $Q[n] = C[n] \cdot m[n]$, which is the quantity of combustion heat released in cycle n. As discussed below, combustion heat release is a readily determined experimental quantity.

In practice we still use Eq. 2 and 3 to simulate cycle-by-cycle combustion, but we recognize that the predicted deterministic behavior follows a one-dimensional mapping. The general appearance of this mapping is illustrated in Fig. 5, which has been constructed by iterating the model twice for different initial cylinder compositions to generate successive combustion heat releases.

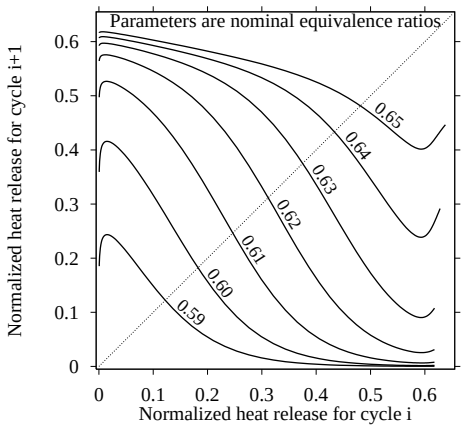

Fig. 5: Mapping functions for various $\phi_\circ$. Fixed parameters were $F = 0.2$, $\phi_\mathrm{l} = 0.57$, $\phi_\mathrm{u} = 0.60$, $\sigma_\phi = \sigma_F = 0$.

3.3 *Stochastic perturbations*

In the remaining part of our model we deal with the higher-dimensional processes. We assume that these other effects can be represented as stochastic fluctuations in one or more key parameters, such as injected fuel-air ratio and residual-gas fraction. By introducing random parameter fluctuations, we intend to account for complex processes such as turbulent mixing, fuel-droplet vaporization, and fuel deposits on the cylinder wall.

We expect that the parametric "noise" will generally appear Gaussian because of the high dimensionality of the processes involved. Thus for each iteration of the model we perturb our parameter values with random Gaussian distributed deviations about the mean (nominal) values. To account for noise in the injection process we perturb the as-injected equivalence ratio, $\phi_\circ$ by

$$\frac{m_\mathrm{new}[n]}{a_\mathrm{new}[n]} = \phi_\circ(1 + \sigma_\phi N(0,1)), \tag{7}$$

where σ_ϕ is a scaling factor and $N(0,1)$ is a zero-mean, unit-variance Gaussian-distributed random deviate determined each cycle. Our experience indicates that typical standard deviation for injection noise is less than 2% of the nominal equivalence ratio.

Likewise we perturb the residual gas fraction, $F_\circ$ on each iterate by

$$F = F_\circ(1 + \sigma_F N(0,1)), \tag{8}$$

where σ_F is a scaling factor and $N(0,1)$ is a zero-mean, unit-variance Gaussian distributed random deviate determined each cycle. Experimental measurements suggest that $F_\circ$ can vary from 0 to 0.3 depending on engine design and operating conditions [15].

4 Model predictions

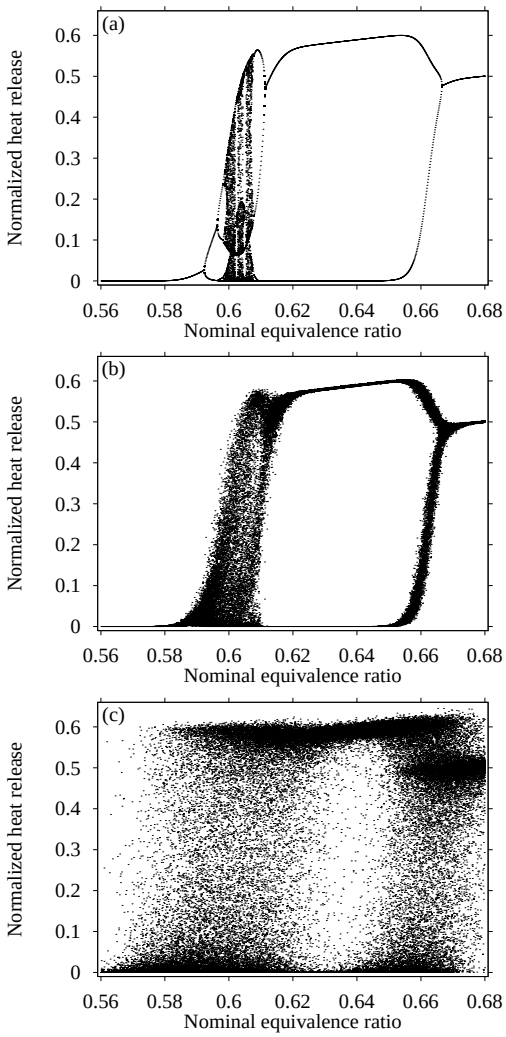

Fig. 6: Model bifurcation plots with $\sigma_\phi = 0$ (a), $\sigma_\phi = 0.001$ (b), and $\sigma_\phi = 0.01$ (c). Fixed model parameters are $\phi_\mathrm{l} = 0.590$, $\phi_\mathrm{u} = 0.595$, $F_\circ = 0.15$ and $\sigma_F = 0$.

Without perturbations to the parameters, our model predicts that cycle-to-cycle combustion will exhibit a period-1 fixed point near stoichiometric fueling and undergo period-doubling bifurcations as the fuel-to-air ratio is reduced. Depending on the specific parameter values selected, the bifurcation sequence may progress to period-2, higher-order periods, or full-blown chaos. At extremely lean fueling the bifurcation reverses and ultimately combustion completely extinguishes. Example bifurcation sequences are shown in Fig. 6 with heat release plotted against as-fed equivalence ratio for various parameter values within expected ranges for real engines.

When parametric perturbations are included, the overall structure of the bifurcation sequences remain, but they become smeared out by the noise as illustrated in Fig. 6. Another important effect of the noise is to cause the onset of bifurcations to begin at higher equivalence ratios and cause the engine to continue running (although very poorly) at extremely lean fueling. Note that the period-1 fixed point continues to be visited frequently well beyond the first period-doubling bifurcation.

5 Experimental

To provide a set of detailed observations which could compared with our model, we measuremented CV in an experimental engine at fueling conditions ranging from near stoichiometric to very lean. Although the engine was highly instrumented, it was basically a production V8 engine with standard port fuel injection connected to a DC motoring dynamometer. Thus we expect that our observations are likely to be commercially relevant.

The nominal engine operating condition was 1200 RPM, 27.1 $\mathrm{N \cdot m}$ brake torque (engine

load), with spark timing fixed at 20 CAD before top center. The dynamometer was operated in speed-control mode to maintain nearly constant engine speed despite erratic combustion at very lean conditions. Feedback engine controllers were initally engaged to achieve an operating condition. Once the steady operation was achieved, the feedback controllers were shut off, and the engine was run in open-loop mode, except for dynamometer speed control. This strategy assured that the observed dynamics reflected combustion rather than the engine controllers.

We recorded combustion pressure each CAD from a single cylinder and nominal operating conditions at a 50 Hz rate for over 2800 contiguous cycles. Combustion pressure measurements were made with a piezo-electric pressure transducer mounted in the cylinder head. To provide a dynamic measurement that could be compared with the model, we calculated the combustion heat release for each cycle by integrating the cylinder pressure data using the Rassweiler-Withrow method [15]. As a result, for each engine experiment we produced time sequences of over 2800 heat-release values.

Although similar CV measurements have been made previously, the experimental protocol described above is not typical. Specifically, we took great care to eliminate non-combustion dynamic effects from the standard engine controllers, and we collected much longer sequences of combustion measurements than is usual. The additional data provided us with much greater confidence in being able to confirm consistent dynamic patterns.

One experimental complication involved the method we used to control fuel-air ratio. Specifically, we controlled injected fuel-air ratio by opening and closing the throttle. Because the throttle changes intake pressure, factors such as in-cylinder mixing and residual gas fraction are also changed. Thus it was not possible to make a series of runs changing only one parameter. Nevertheless, we were able to vary the degree of CV enormously from very small amounts near stoichiometric fueling ($\phi_\circ = 1.0$) to very high amounts at very lean fueling ($\phi_\circ < 0.55$).

6 Application of symbol-sequence statistics

Contending with the effects of dynamical parameter noise is a key issue in characterizing the predicted model dynamics and comparing the model with experimental observations. As demonstrated by the model bifurcation diagrams, we expect such noise to blur but not completely obscure the deterministic signature. One technique we have found to be very useful in observing these noisy dynamical patterns is the symbol-sequence approach suggested by Tang *et al.* [16]. We use symbol sequences to both depict and compare dynamic patterns in observed or model-produced measurements.

The basic idea in data symbolization is to discretize the predicted or measured heat release values into n possible values. Depending on the value of a given heat release, it is assigned one of n symbolic values (*e.g.*, "0" or "1" for a binary partition). A key constraint we employ is to define discretization partitions such that the individual occurrence of each symbol is equiprobable with all others.

Once a heat-release time series is discretized, we evaluate the relative frequency of all possible symbol sequences in the data defined by a symbol vector of m cycles length. For

example, if we let $m = 5$, we determine the relative frequency of occurrence for each possible sequential combination of 5 symbols. In this sense, the parameter m is like an embedding dimension; Tang *et al.* refer to m as the *number of tree levels*.

A simple way for keeping track of symbol-sequence frequencies is to assign a unique bin number to each possible sequence by evaluating the equivalent decimal value of each base-n sequence; we term this the *sequence code*. For example, a sequence of "010101" occurring with a binary partition ($n = 2$) and a 6-level tree ($m = 6$) would be assigned a bin number of 21. This is very similar to the approach used by White and Rechester [17]. Using this method of identifying each symbol sequence also allows us to observe the relative-frequency histograms as two-dimensional plots (see Section 7).

We refer to the tally of symbol-sequence frequencies vs. sequence bin number as a *symbol-sequence histogram*. Because of our partitioning rule, the relative frequencies for truly random data will all be equal, and all histogram bins will be equally probable (subject to the availability of sufficient data). Thus any significant deviation from equiprobability is indicative of some kind of time correlation and deterministic structure. Similar to Tang *et al.*, we define a modified Shannon entropy as:

$$H_S(m) \equiv \frac{1}{\log n^{\text{seq}}} \sum_i p_{i,m} \log p_{i,m} \tag{9}$$

where n^{seq} is the total number of observed sequences (*i.e.*, the number of bins with non-zero frequency), i is a string-sequence index of tree depth m, and $p_{i,m}$ is the probability of string sequence i. The only difference between Eq. 9 and the definition used by Tang *et al.* is that we use the number of nonempty bins rather than the total number of possible sequences. For random data H_S should equal 1, whereas for nonrandom data it should be between 0 and 1. In the current context, lower H_S implies more deterministic structure.

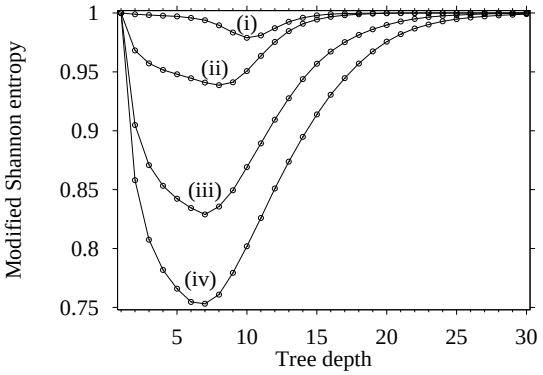

Fig. 7: Modified Shannon entropy with a binary partition as a function of tree depth for the model at four equivalence ratios ($\phi_\circ$): 0.91 (i), 0.67 (ii), 0.63 (iii) and 0.59 (iv).

One approach we have found useful for selecting an appropriate sequence vector length (m) involves using the modified Shannon entropy. Specifically, we find that H_S typically reaches a minimum value as vector length is increased from 1. This trend is illustrated in Fig. 7 using noisy data generated with our engine model. As the bifurcation progresses, the nonrandom part of the engine model becomes more evident, even though significant parameter noise is present. We explain this minimum in H_S as reflecting the symbol-sequence transformation which best distinguishes the data from a random sequence. Sequence vectors that are too short lose some of the important deterministic information. Sequence vectors that are too long reflect noise and data depletion (*i.e.*, there is not enough data to get reliable statistics for such long sequences). Thus one can argue that the m value for which H_S is minimum is an "optimal" choice for the given data.

7 Symbol-sequence comparisons

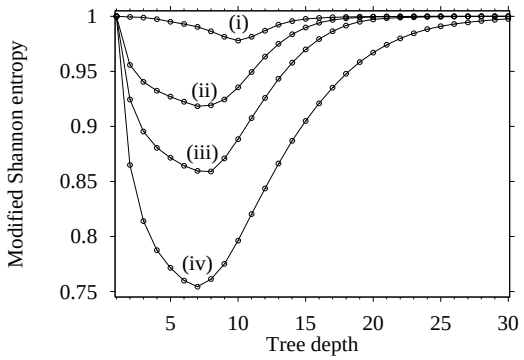

Fig. 8: Modified Shannon entropy with a binary partition as a function of tree depth for engine data at four equivalence ratios ($\phi_\circ$): 0.91 (i), 0.67 (ii), 0.63 (iii) and 0.59 (iv).

In comparing the model and experimental heat-release patterns, we begin by evaluating the general trends for the modified Shannon entropy. As illustrated in Fig. 8, we find that the real engine exhibited similar trends in H_S with degree of leanness in fueling and symbol sequence length (compare with Fig. 7 for the model). This similarity suggests that the model and real engine are at least roughly similar in their degree of time correlation and response to lean fueling.

Fig. 9 illustrates a more detailed comparison of the model and experiment through a sequence of two-dimensional symbol-sequence histograms. The horizontal axis for all plots is designated in terms of the decimal equivalent of the six-member binary sequence (*i.e.*, $n = 2$, $m = 6$). Note that in both cases, peaks reflecting high frequencies of "010101" (21) and "101010" (42) combinations begin to emerge from a flat profile as the noisy period-2 bifurcation begins. The high visibility of these peaks, even when there is a large amount of noise, suggests that symbol-sequence histograms may be generally useful for detecting the onset of noisy bifurcations.

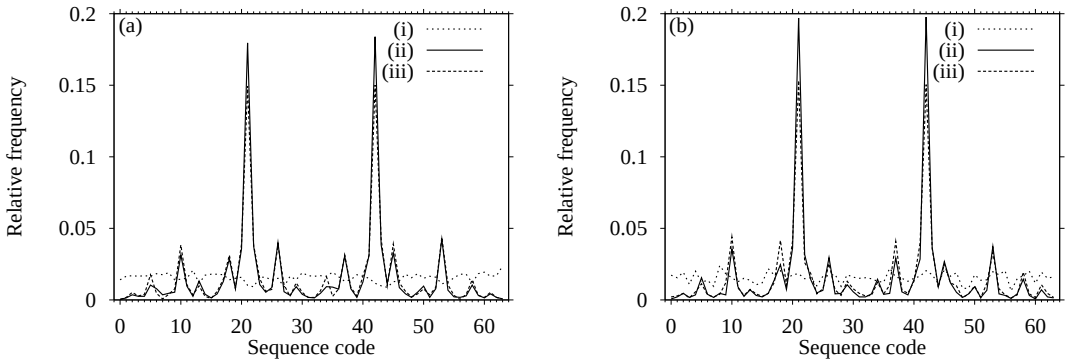

Fig. 9: Symbol-sequence histograms with six-member binary sequences for model (a) and engine (b) at three equivalence ratios ($\phi_\circ$): 0.91 (i), 0.59 (ii), and 0.53 (iii).

8 Fitting the model

As mentioned previously, we were not able to control our experimental engine such that all of the parameters remained constant while the injected fuel-air ratio was reduced. We also had no way of directly measuring the residual fraction, $F_\circ$, or the noise amplitudes for $F_\circ$ and the injected fuel-air ratio, $\phi_\circ$. Thus in comparing the model and experiment in detail, we were limited to evaluating how well the model could reproduce the observed behavior as the unknown parameters were adjusted over physically reasonable ranges.

To fit the model against observed data, we adjusted the model free parameters, ϕ_{l}, ϕ_{u}, $\phi_{\circ}$, σ_{ϕ}, $F_{\circ}$, σ_F and a multiplicative scale factor relating nondimensional to experimental heat release units. We modeled stochastic parameter perturbations with multiplicative white Gaussian noise. We optimized the fit by iteratively adjusting the parameters to give the best agreement between symbol stream statistics (as represented by the symbol-sequence histogram) for iterations of the model and experimental data.

We use acceptance probability of the two-sample chi-squared statistic as the criterion for minimization:

$$\chi^2 \equiv \sum_i \frac{(N_i^{\mathrm{obs}} - N_i^{\mathrm{model}})^2}{N_i^{\mathrm{obs}} + N_i^{\mathrm{model}}} \tag{10}$$

Using this method, we can also evaluate the statistical significance of a trial model fit, using the standard χ^2 probability inference with $N^{\mathrm{bins}} - 1$ degrees of freedom, with N^{bins} the total number of bins with non-zero occupation for either model or data. The minimization statistic in [16] was the Euclidean distance between vectors whose elements are the occupations of all the bins, which resembles Eq. 10 without the denominator term.

With a good fit, the model converges to a χ^2 value which will accept the null hypothesis that the same process generated the bin occupations for model and experiment, thus confirming that the model quantitatively mimics the experimental observations in some detail. The minimization algorithm [18] was a hybrid of simplex and genetic methods designed for continuous parameter spaces without requiring derivatives.

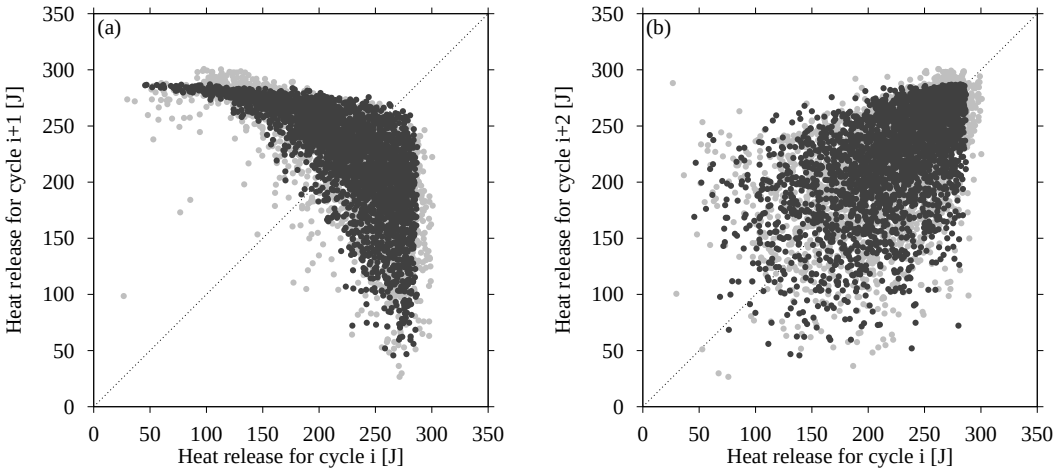

Fig. 10: Lag-1 (a) and lag-2 (b) return maps for engine data at $\phi_{\circ} = 0.59$ (light points) and optimized-fit model data (dark points).

Whereas a binary partition is quite sufficient for detecting the onset of bifurcations, we find that higher-level partitions are needed for accurate fits of our engine model to experimental data. In Fig. 10a we illustrate how well the fitted model first return map matches the observed first return map for a moderately lean fueling case. The agreement is equally close when the lag-2 return maps are compared as in Fig. 10b. We used a variable partition of 9 and 8 in a 2-cycle-long sequence to achieve this degree of fit, where 9 is the number of partitions applied to the first member of the sequence and 8 is the number of partitions used for the second member.

Note that in the first return map comparison (Fig. 10a), there is a downward bias in the upper-left portion of the experimental map. This bias is a consistently occurring feature that we expect is due to a real difference between our model and the experimental engine. We attribute this to an additional temperature effect that is currently unaccounted for by the model. Specifically, we conjecture that lower-than-expected heat release occurs following exceptionally poor combustion events because of reduced initial temperature at the time of spark. We plan to include this reduced temperature effect in future revisions of our model.

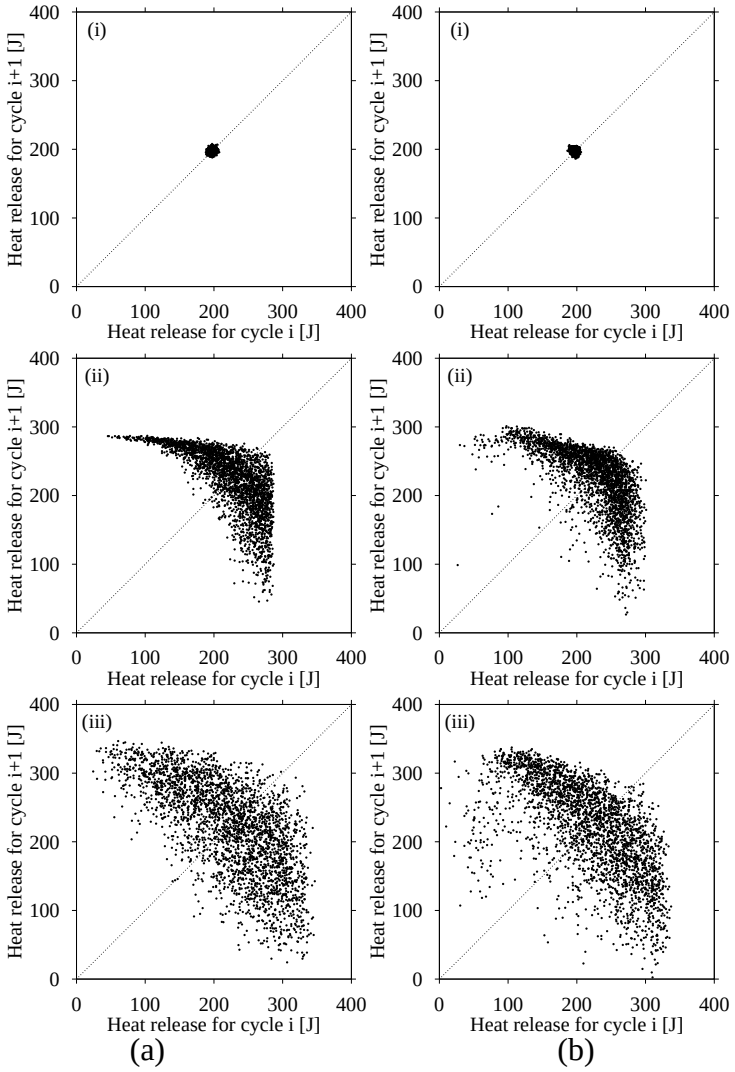

Fig. 11: Return maps for model (a) and engine (b) at three equivalence ratios ($\phi_\circ$): 0.91 (i), 0.59 (ii) and 0.53 (iii).

Finally, in Fig. 11, we illustrate how well the general trends of the model and experimental data match. At each of three fueling conditions corresponding to near stoichiometric, moderately lean, and very lean, we fitted the model to the observed data. It is apparent that the same basic patterns are clearly occurring in both cases; namely a transition from 1) very-small-amplitude Gaussian combustion variation near stoichiometric fueling to 2) a noisy period-2 combustion bifurcation at moderately lean fueling to 3) a noisy multi-period (possibly chaotic) combustion condition at the leanest condition. For all three fueling conditions the fitted parameter values are well within the range of physical plausibility. The model is specific enough that there is little chance that such similar trends could be caused by overfitting an overly general and unrealistic mathematical function.

9 Conclusions

Our model provides a physically reasonable hypothesis that explains the observed time-resolved *patterns* in cyclic combustion variability. Depending on injected fuel-air ratio, the behavior can appear to be purely stochastic or a mixture of stochastic and nonlinear dynamics. This range of possible behavior may explain apparently conflicting observations from previous studies. The ability to describe engine fluctuations with such a simple yet physically plausible model may also aid in the development of cycle-resolved control to reduce or alter the pattern of cyclic fluctuations in order to improve engine performance.

Symbol-sequence statistics provide a useful tool for characterizing and comparing noisy nonlinear dynamics similar to what we observed. Specific promising applications include the detection of bifurcations and the fitting of models against data.

10 Acknowledgements

This work is supported by the U.S. Department of Energy, Office of Energy Research and Ford Motor Company.

11 References

[1] D. Clerk, *The Gas Engine* (Longmans, Green & Co., 1886).
[2] R.K. Barton, D.K. Kenemuth, S.S. Lestz, W.E. Meyer, SAE Paper No. 700488 (1970).
[3] J.C. Kantor, Science **224**, 1233 (1984).
[4] M.R. Belmont, M.S. Hancock, D.J. Buckingham, SAE Paper No. 860324 (1986).
[5] J.W. Daily, Combust. Sci. & Tech. **57**, 149 (1988).
[6] J.K. Martin, S.L. Plee, D.J. Remboski, Jr., SAE Paper No. 880201 (1988).
[7] Y. Moriyoshi, T. Kanimoto, M. Yagita, SAE Paper No. 930066 (1993).
[8] G. Grünefeld, V. Beushausen, P. Andresen, W. Hentschel, SAE Paper No. 941880 (1994).
[9] C. Letellier, S. Meunier-Guttin-Cluzel, G. Gouesbet, F. Neveu, T. Duverger, B. Cousyn, SAE Paper No. 971640 (1997).
[10] C.E.A. Finney, K. Nguyen, C.S. Daw, in *Proceedings of the 32nd Japanese Symposium on Combustion, 1994*, p. 400.
[11] M.B. Young, SAE Paper No. 810020 (1981).
[12] N. Ozdor, M. Dulger, E. Sher, SAE Paper No. 940987 (1994).
[13] C.S. Daw, C.E.A. Finney, J.B. Green, Jr., M.B. Kennel, J.F. Thomas, F.T. Connolly, SAE Paper No. 962086 (1996).
[14] I. Glassman, *Combustion* (Academic Press, 1987), 2nd ed.
[15] J.B. Heywood, *Internal Combustion Engine Fundamentals* (McGraw-Hill, 1988).
[16] X.Z. Tang, E.R. Tracy, A.D. Boozer, A. deBrauw, R. Brown, Phys. Rev. E **51**, 3871 (1995); X.Z. Tang, E.R. Tracy, A.D. Boozer, A. deBrauw, R. Brown, Phys. Lett. A **190**, 393 (1994).
[17] A.B. Rechester, R.B. White, Phys. Lett. A **156**, 419 (1991); *ibid.* **158**, 51 (1991).
[18] R. Storn, K. Price, International Computer Science Institute Technical Report TR-95-012, 1995 (unpublished). Available at ftp://ftp.icsi.berkeley.edu.